PROCEEDINGS OF SCIENCE

CALET's sensitivity to electron cosmic-ray spectral and anisotropy signatures of the Vela SNR

Holger Motz[a,*] **for the CALET collaboration**

[a] *Waseda University, Faculty of Science and Engineering, Global Center for Science and Engineering Okubo 3-4-1, Shinjuku, Tokyo, Japan*

E-mail: motz@aoni.waseda.jp

The ISS-based Calorimetric Electron Telescope (CALET) is directly measuring energy and arrival direction of electron+positron cosmic rays (CR) well into the TeV region. Due to energy loss in propagation, TeV-range CR electrons are expected to originate from only a few nearby and young supernova remnants (SNRs), foremost the Vela SNR, potentially giving rise to spectral features and flux anisotropy as signatures. To further CALET's goal of finding a signature of Vela, a novel non-binned analysis algorithm quantifying the significance of a potential spectral hardening in the TeV region from the near-SNR contribution was developed, as well as an analysis method for anisotropy which enhances the signature significance by fixing the dipole axis towards the Vela SNR. The sensitivity of CALET to these spectral and anisotropy signatures was evaluated by using the new analysis methods on simulated event samples based on an interpretation model fitted to the currently measured electron and positron spectra. In addition to an explanation of the analysis methods, the expected significance of the spectral and anisotropy signatures as well as their combination are presented for a selection of representative conditions for the emission of electron CR by the nearby SNRs.

39th International Cosmic Ray Conference (ICRC2025)
15–24 July 2025
Geneva, Switzerland

*Speaker

PoS(ICRC2025)099

1. Introduction

The electron+positron cosmic-ray flux in the TeV energy region is expected to originate primarily from very nearby supernova remnants (SNR), since radiative energy loss limits the propagation distance of electron cosmic rays reaching Earth at TeV energy to less than one kiloparsec (kpc) [1]. A softening of the all-electron spectrum around one TeV [2] corroborates the assumption that a transition from many distant to few nearby sources takes place at this energy. Three SNRs are likely sources for the TeV range flux: The Vela SNR is expected to dominate the spectrum in the TeV region due to its distance of $\sim$ 0.3 kpc and age of $\sim$ 11 kyr, while the Monogem SNR with also $\sim$ 0.3 kpc distance but an age of $\sim$ 86 kyr may give a contribution at the lower end of the TeV region, and Cygnus Loop with a larger distance of $\sim$ 0.44 kpc and $\sim$ 20 kyr could give a smaller contribution in a similar energy range as Vela. The contribution of these individual sources depends especially on the timing of the cosmic-ray emission after the supernova explosion and the maximum energy of their source spectrum, and depending on these parameters their contribution could cause a re-hardening of the observed spectrum at several TeV. While this signature of an individual source would be observed in the spectrum, anisotropy in arrival direction is another possible effect of a dominating single nearby source, as there would be a gradient in the cosmic-ray density pointing towards the source. An un-binned spectral fit tuned to the re-hardening signature and an analysis method focusing on the direction towards Vela in order to enhance the sensitivity over general analysis methods have been developed. The probability to achieve a 5σ detection of a signature for CR emission from Vela with this analysis method was studied for a range of condition of emission timing and spectrum cutoff, both for the data already taken up to the end of 2023 and for the data expected to be taken by 2030, the end of the currently approved mission extension of CALET.

2. Un-binned Spectral Fit

To improve the sensitivity to the re-hardening of the spectrum over a fit to the binned spectrum where information is lost in binning process, an un-binned fit working directly on the list of event energies was developed. The distribution of event energies is fitted by minimizing -log(L) where likelihood L is the product of the probability density function (PDF)

$$PDF = (1-a)E^{-\gamma_1} e^{-\left(\frac{E}{E_c}\right)} + aE^{-\gamma_2} \tag{1}$$

over all events. The first cut-off power-law term represents the contribution from distant SNR, while the second power law term represents the nearby SNR. The PDF is normalized by the complementary cumulative distribution function (CCDF)

$$CCDF = (1-a)\left(E_c^{1-\gamma_1}\Gamma_{inc}\left(1-\gamma_1, \frac{E}{E_c}\right)\right) + a\left(\frac{E^{1-\gamma_2}}{1-\gamma_2}\right) \tag{2}$$

in which Γ_{inc} is the incomplete gamma function. The availability of a closed form expression for the CCDF is one reason Eq. 1 was chosen over other possible PDF functions such as a double soft broken power-law, since numerical integration does not provide a sufficiently precise normalization for a stable minimization. The fitting is performed with a modified version of the python package Powerlaw [3]. The significance of the existence of the extra power-law term for the nearby SNR

sources is determined from the ratio to the likelihood calculated for the base-model without the extra power-law term, for which the PDF is given by:

$$PDF = E^{-\gamma_1} e^{-\left(\frac{E}{E_C}\right)} \tag{3}$$

The significance σ is determined from the χ^2 distribution for two additional degrees of freedom related to the likelihood ratio by Wilks' theorem $-2\Delta\log(L) \approx \chi^2$ [4].

3. Directional Anisotropy Analysis

An omni-directional search for a dipole anisotropy as described in Ref. [5] has three degrees of freedom, the dipole's direction encoded by two angles and the dipole amplitude. To test the hypothesis of a dipole anisotropy caused by Vela we can restrict our search to the known direction towards the source, leaving only one degree of freedom, which increases sensitivity. The analysis is designed to yield a likelihood-ratio, which can be combined with that of the spectral fit by multiplication. The likelihood is calculated as $L = \prod_i L_i$ where i loops over the pixels of a nside=64 healpix map, with $L_i = e^{-\mu_i}\frac{\mu_i^{n_i}}{n_i!}$ being the Poisson statistics probability for μ_i expected and n_i measured events in pixel i. The expected number of events as a sky-map is given by

$$\mu = (M + \delta \times D) \times A \times \frac{\sum n_i}{\sum A_i} \tag{4}$$

where M is the monopole map (isotropic sphere) and D is the dipole map towards Vela, i.e. $\cos\Theta$ where Θ is the angle from Vela direction and A the exposure map. By minimizing -log(L) with δ as free parameter, the best fit dipole amplitude δ_{BF} is obtained, from which the likelihood ratio $L(\delta = \delta_{BF})/L(\delta = 0)$ is calculated. As the minimium energy of the event sample, each event's energy is used in turn, from the highest down to 300 GeV, and the average likelihood ratio taken, which reduces the influence of white noise fluctuation. From the averaged likelihood ratio, the significance is calculated via Wilks' theorem and the χ^2 distribution for one degree of freedom. The combined significance for spectral and anisotropy signal is calculated by multiplication of the likelihood ratios and using the χ^2 distribution for two degrees of freedom which is the larger value from the two involved likelihood ratio tests.

4. Flux Modeling and Sample Creation

The modeled electron and positron flux is comprised of a component for the distant SNRs, parameterized as a broken power law with exponential cut-off (electron), a semi-analytically calculated contribution from the pulsars listed in the ATNF catalog [6] (electron and positron), secondary particle flux taken from DRAGON [7] calculations of nuclei propagation (electron and positron), as well as the electron flux from the nearby SNRs, which are calculated with DRAGON. This modeling and the fit to CALET all-electron data [2] and AMS-02 positron-only data [8] are described in detail in in Ref. [9], though the propagation model published in Ref. [10] is used.

Fig. 1 shows the best fit results for two representative conditions, a 5000 yr delay of the CR release with a spectral cut-off at 10 TeV under the assumption that Vela dominates the TeV-region spectrum (i.e. the contributions from Cygnus Loop and Monogem are ignored), ("Model

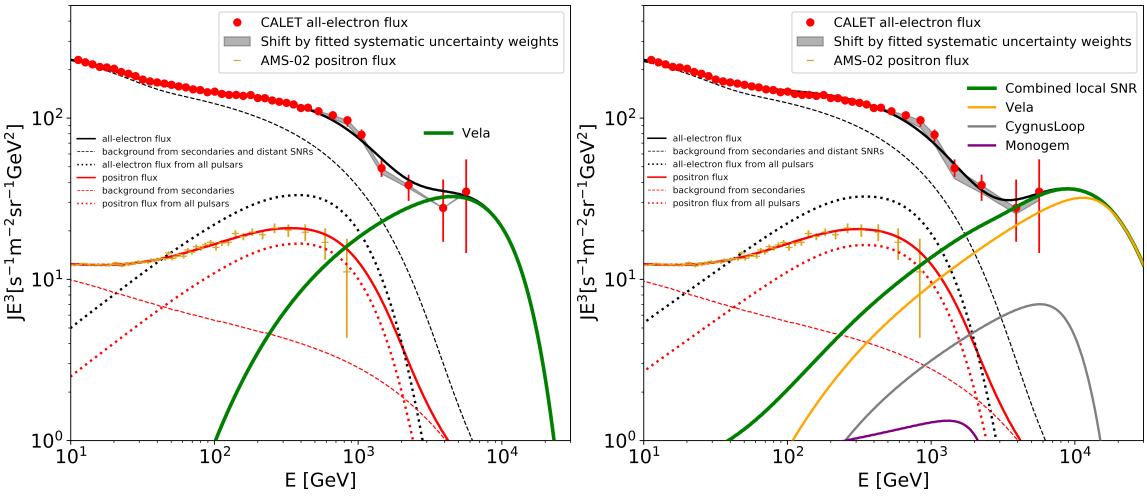

Figure 1: Example fits to CALET all-electron and AMS-02 positron-only data, for 5000 yr delay, 10 TeV cut-off, Vela only case (left: Model A) and 10000 yr duration, 100 TeV cut-off, three nearby SNR case (right: Model B)

A" hereafter) and 10000 yr continuous emission of CR with a spectral cut-off at 100 TeV with contributions from all three nearby SNRs included ("Model B" hereafter). For the best fit flux of each condition, 1000 samples of simulated CALET event data with a randomized energy and direction distribution are created. The direction distribution is based on the flux anisotropy from the nearby SNRs which is extracted from the result of the propagation calculation with DRAGON, assuming the background from distant SNRs and pulsars to be isotropic. Furthermore, the energy-dependent exposure map of the CALET detector for the observation period from start of observation in October 2015 to the end of 2023 is applied as a weight, to take the uneven exposure to different regions of the sky into account. The total exposure determining the event numbers and energy distribution is also taken from these maps, with the exposure multiplied by 1.8 in the creation of 1000 additional samples for simulation of the extended observation until 2030.

5. Results

Using the spectral fit and anisotropy analysis on the 1000 samples created for each condition yields distributions of the detection significance. For the spectral fit, it was found that a 5σ level is obtainable in many cases, while for the anisotropy analysis only 2σ is a viable threshold. However, its combination with the spectral fit may improve the chance of reaching 5σ. Fig. 2 shows these distributions for Model A and Fig. 3 for Model B. The probability of reaching 5σ with the spectral fit and the combined analysis under each studied condition is listed in Table 1 for the Vela-only case and in Table 2 for the case of three nearby SNR. The probability of reaching 2σ with the directional anisotropy analysis and the increase in probability for a 5σ detection if combining the anisotropy signal with the spectral fit are shown in Table 3 (Vela-only) and in Table 4 (three nearby SNR). Model B shows the largest improvement of 22.5% among all tested conditions.

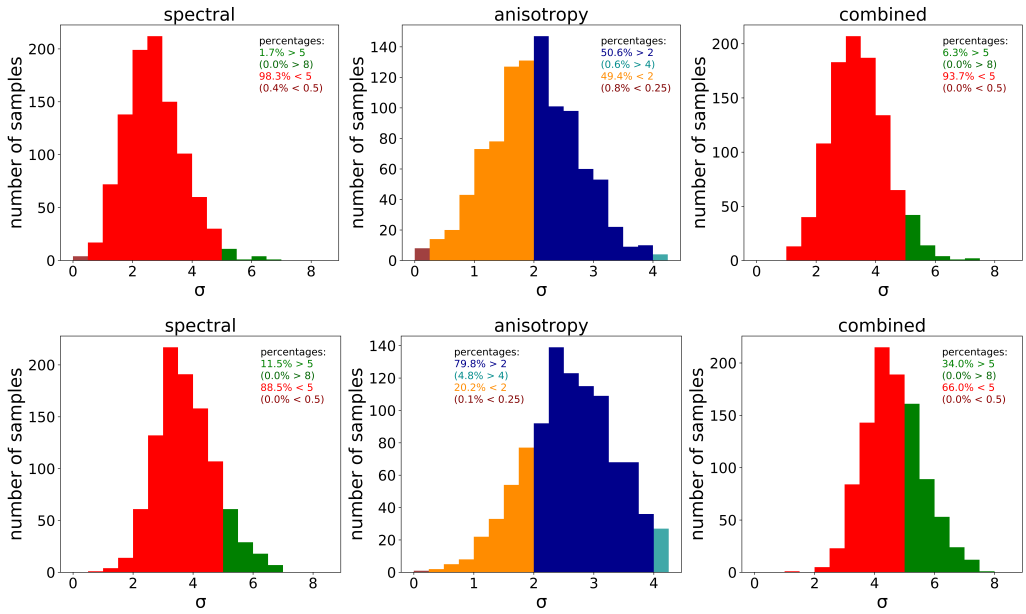

Figure 2: Example sensitivity distributions for Model A, for spectral fit (left), anisotropy analysis (center) and combined analysis (right). The upper panel shows the results for observation until 2023, the lower one until 2030.

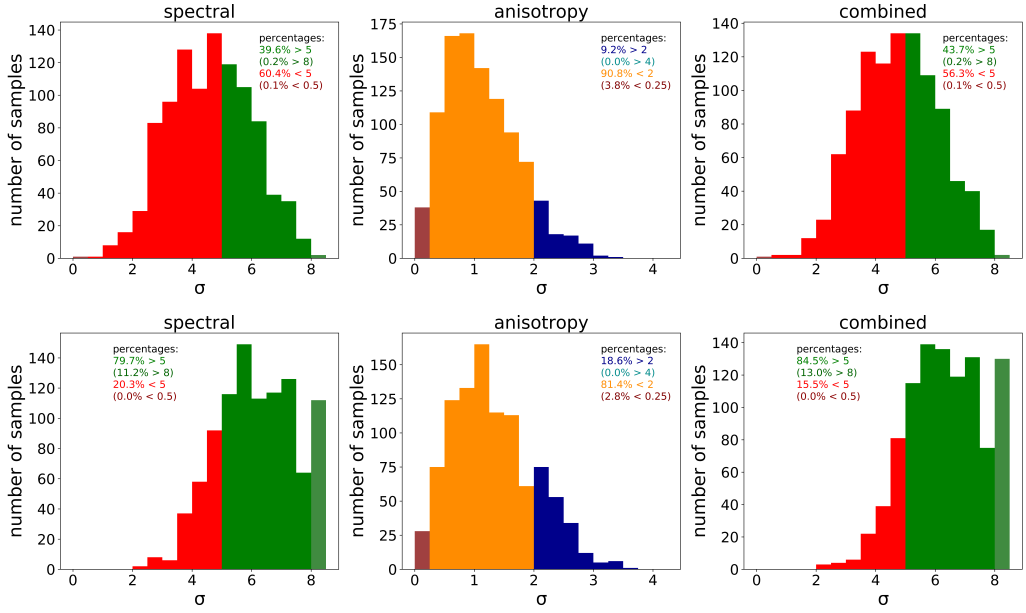

Figure 3: Example sensitivity distributions for Model B, for spectral fit (left), anisotropy analysis (center) and combined analysis (right). The upper panel shows the results for observation until 2023, the lower one until 2030.

Table 1: Probabilities for 5σ significance for the Vela-only case depending on injection timing (rows) and injection spectrum cut-off (columns). Upper line in each cell gives the values for the observation until 2023, lower line the values for observation until 2030. The left value in each line is the probability from spectral fit only, the right value for the combined spectral-anisotropy analysis.

	$E_{cut} = 10$ TeV	$E_{cut} = 20$ TeV	$E_{cut} = 50$ TeV	$E_{cut} = 100$ TeV
instant emission	0.2% | 0.6% 1.8% | 8.7%	3.3% | 5.1% 20.4% | 32.1%	14.2% | 18.2% 55.6% | 65.1%	23.5% | 28.3% 71.5% | 79.2%
2500 yr duration	0.6% | 1.3% 2.3% | 12.1%	2.8% | 6.1% 23.1% | 34.4%	20.6% | 24.8% 66.5% | 73.7%	31.2% | 37.3% 77.2% | 84.0%
5000 yr duration	0.3% | 1.0% 2.1% | 8.4%	8.3% | 12.1% 34.9% | 49.2%	26.7% | 33.3% 73.6% | 81.2%	25.4% | 31.0% 70.1% | 77.6%
7500 yr duration	1.8% | 3.4% 6.8% | 18.4%	12.1% | 18.6% 45.5% | 58.3%	34.8% | 39.7% 79.0% | 84.9%	45.0% | 51.7% 87.4% | 91.8%
10000 yr duration	2.6% | 6.6% 14.7% | 36.3%	20.8% | 26.9% 62.2% | 74.4%	42.1% | 49.3% 85.1% | 90.4%	53.4% | 59.0% 89.7% | 93.3%
2500 yr delay	0.5% | 1.9% 4.6% | 13.8%	5.6% | 9.4% 31.2% | 44.0%	25.4% | 31.4% 70.1% | 77.7%	32.4% | 37.9% 80.6% | 85.9%
5000 yr delay	1.7% | 6.3% 11.5% | 34.0%	22.9% | 32.1% 66.2% | 78.5%	42.4% | 50.3% 86.0% | 92.1%	55.8% | 63.7% 92.3% | 95.8%
7500 yr delay	5.8% | 9.4% 24.3% | 44.8%	26.7% | 34.0% 68.0% | 79.7%	42.8% | 50.3% 86.2% | 91.0%	67.3% | 72.5% 93.9% | 96.5%
10000 yr delay	26.3% | 33.3% 67.6% | 80.9%	49.7% | 57.2% 88.8% | 93.8%	69.7% | 74.6% 97.3% | 98.9%	74.5% | 79.2% 96.8% | 98.3%

Table 2: Probabilities for 5σ significance for the case of three nearby SNRs depending on injection timing (rows) and injection spectrum cut-off (columns). Upper line in each cell gives the values for the observation until 2023, lower line the values for observation until 2030. The left value in each line is the probability from spectral fit only, the right value for the combined spectral-anisotropy analysis.

	$E_{cut} = 10$ TeV	$E_{cut} = 20$ TeV	$E_{cut} = 50$ TeV	$E_{cut} = 100$ TeV
instant emission	0.1% | 0.1% 0.7% | 2.0%	1.9% | 2.3% 12.4% | 16.4%	5.2% | 6.3% 26.5% | 32.9%	14.7% | 17.3% 50.2% | 55.9%
2500 yr duration	0.0% | 0.0% 1.1% | 2.9%	3.1% | 4.5% 13.1% | 17.8%	9.4% | 12.1% 43.1% | 49.3%	17.7% | 21.3% 59.0% | 64.0%
5000 yr duration	0.1% | 0.5% 1.4% | 4.1%	2.6% | 3.9% 19.2% | 25.4%	14.7% | 16.8% 48.8% | 54.8%	26.3% | 29.0% 67.8% | 72.4%
7500 yr duration	0.5% | 1.1% 4.3% | 7.8%	4.0% | 5.9% 21.6% | 28.6%	21.7% | 26.0% 66.2% | 71.3%	29.9% | 31.7% 75.0% | 79.3%
10000 yr duration	0.5% | 0.8% 5.3% | 9.4%	6.8% | 8.5% 29.6% | 37.8%	27.2% | 31.7% 71.3% | 77.0%	39.6% | 43.7% 79.7% | 84.5%
2500 yr delay	0.1% | 0.2% 1.7% | 3.8%	4.3% | 6.0% 21.9% | 28.3%	13.4% | 15.9% 49.3% | 55.4%	19.1% | 23.0% 65.3% | 69.9%
5000 yr delay	0.9% | 1.8% 5.1% | 10.9%	7.7% | 10.7% 34.5% | 44.3%	32.8% | 37.0% 76.7% | 80.5%	40.0% | 44.7% 84.8% | 88.8%
7500 yr delay	3.3% | 4.9% 19.7% | 31.2%	19.4% | 23.2% 55.8% | 64.0%	43.1% | 47.4% 79.4% | 83.8%	50.0% | 53.1% 85.2% | 88.5%
10000 yr delay	3.9% | 4.5% 18.4% | 20.3%	23.5% | 26.1% 67.2% | 69.2%	40.9% | 41.9% 82.8% | 83.5%	50.0% | 52.1% 84.9% | 85.5%

Table 3: Results of the anisotropy analysis in the Vela-only case depending on injection timing (rows) and injection spectrum cut-off (columns). Upper line in each cell gives the values for the observation until 2023, lower line the values for observation until 2030. The left value in each line is the probability from the anisotropy analysis, while the right value shows the increase in probability for a 5σ detection which the addition of the anisotropy analysis provides to the spectral fit.

	$E_{cut} = 10$ TeV	$E_{cut} = 20$ TeV	$E_{cut} = 50$ TeV	$E_{cut} = 100$ TeV
instant emission	24.6% | 0.4% 48.2% | 6.9%	16.9% | 1.8% 33.0% | 11.7%	14.3% | 4.0% 26.9% | 9.5%	15.2% | 4.8% 23.4% | 7.7%
2500 yr duration	28.4% | 0.7% 51.1% | 9.8%	18.8% | 3.3% 35.9% | 11.3%	15.6% | 4.2% 28.2% | 7.2%	13.3% | 6.1% 25.9% | 6.8%
5000 yr duration	33.5% | 0.7% 59.3% | 6.3%	22.8% | 3.8% 41.3% | 14.3%	17.7% | 6.6% 33.2% | 7.6%	16.8% | 5.6% 29.5% | 7.5%
7500 yr duration	29.1% | 1.6% 50.8% | 11.6%	28.5% | 6.5% 44.4% | 12.8%	20.2% | 4.9% 40.5% | 5.9%	19.9% | 6.7% 33.3% | 4.4%
10000 yr duration	38.3% | 4.0% 70.4% | 21.6%	26.9% | 6.1% 45.9% | 12.2%	22.5% | 7.2% 40.1% | 5.3%	20.3% | 5.6% 37.7% | 3.6%
2500 yr delay	29.8% | 1.4% 51.0% | 9.2%	21.7% | 3.8% 38.7% | 12.8%	18.8% | 6.0% 31.8% | 7.6%	16.7% | 5.5% 28.9% | 5.3%
5000 yr delay	50.6% | 4.6% 79.8% | 22.5%	32.6% | 9.2% 55.3% | 12.3%	25.1% | 7.9% 44.4% | 6.1%	23.0% | 7.9% 42.7% | 3.5%
7500 yr delay	42.7% | 3.6% 69.3% | 20.5%	34.4% | 7.3% 59.5% | 11.7%	21.4% | 7.5% 40.4% | 4.8%	24.4% | 5.2% 44.3% | 2.6%
10000 yr delay	31.9% | 7.0% 58.0% | 13.3%	26.5% | 7.5% 47.6% | 5.0%	20.3% | 4.9% 41.9% | 1.6%	19.7% | 4.7% 37.7% | 1.5%

Table 4: Results of the anisotropy analysis in the case of three nearby SNRs depending on injection timing (rows) and injection spectrum cut-off (columns). Upper line in each cell gives the values for the observation until 2023, lower line the values for observation until 2030. The left value in each line is the probability from the anisotropy analysis, while the right value shows the increase in probability for a 5σ detection which the addition of the anisotropy analysis provides to the spectral fit.

	$E_{cut} = 10$ TeV	$E_{cut} = 20$ TeV	$E_{cut} = 50$ TeV	$E_{cut} = 100$ TeV
instant emission	10.0% | 0.0% 19.5% | 1.3%	7.7% | 0.4% 12.8% | 4.0%	7.5% | 1.1% 11.8% | 6.4%	6.6% | 2.6% 11.5% | 5.7%
2500 yr duration	12.2% | 0.0% 24.4% | 1.8%	8.2% | 1.4% 15.0% | 4.7%	7.8% | 2.7% 14.0% | 6.2%	6.9% | 3.6% 11.2% | 5.0%
5000 yr duration	14.7% | 0.4% 28.7% | 2.7%	10.9% | 1.3% 18.5% | 6.2%	9.1% | 2.1% 14.8% | 6.0%	6.6% | 2.7% 12.3% | 4.6%
7500 yr duration	18.0% | 0.6% 31.5% | 3.5%	11.4% | 1.9% 20.5% | 7.0%	10.9% | 4.3% 18.4% | 5.1%	7.7% | 1.8% 14.4% | 4.3%
10000 yr duration	14.5% | 0.3% 30.3% | 4.1%	11.7% | 1.7% 21.2% | 8.2%	10.2% | 4.5% 16.4% | 5.7%	9.2% | 4.1% 18.6% | 4.8%
2500 yr delay	13.7% | 0.1% 24.9% | 2.1%	10.6% | 1.7% 19.2% | 6.4%	8.4% | 2.5% 13.9% | 6.1%	9.3% | 3.9% 13.1% | 4.6%
5000 yr delay	18.2% | 0.9% 32.8% | 5.8%	12.3% | 3.0% 26.5% | 9.8%	12.3% | 4.2% 21.5% | 3.8%	11.1% | 4.7% 19.5% | 4.0%
7500 yr delay	19.3% | 1.6% 31.9% | 11.5%	15.2% | 3.8% 26.3% | 8.2%	12.6% | 4.3% 20.1% | 4.4%	10.6% | 3.1% 19.5% | 3.3%
10000 yr delay	3.0% | 0.6% 5.5% | 1.9%	3.1% | 2.6% 5.0% | 2.0%	3.2% | 1.0% 4.7% | 0.7%	3.6% | 2.1% 3.9% | 0.6%

6. Discussion and Conclusion

Newly developed un-binned spectral fit and directional anisotropy analysis methods have been evaluated, giving sensitivity estimates for detection of a signature of the Vela SNR by CALET observation as performed until 2023 and extrapolated until 2030. It is shown that depending on the injection parameters there is a high probability of a 5σ discovery of the combined spectral-anisotropy signature. Inclusion of the anisotropy signature raises the probability by up to 22.5% (11.5%) and by 9.0% (4.7%) on average for the case of Vela dominating (three nearby SNRs contributing to) the TeV-region spectrum, for observation until 2030. Comparing the results for observation until 2023 and until 2030, it is found that the additional observation time would greatly increase the chances of discovery, with a maximum increase by 48.2% (46.2%) and an average increase by 30.0% (26.7%). While further verification of the exposure function is needed before this method is applied on flight data, the presented sensitivity study shows its potential for enabling discovery of a Vela signature and underscores the importance of continued data-taking with CALET.

Acknowledgements

We gratefully acknowledge JAXA's contributions to the development of CALET and to the operations aboard the JEM-EF on the ISS. This work was supported in part by JSPS Grant-in-Aid for Scientific Research (S) No. 26220708, No. 19H05608, and No. 24H00025, JSPS Grant-in-Aid for Scientific Research (B) No. 24K00665, and by the MEXT Supported Program for the Strategic Research Foundation at Private Universities (2011-2015) (No. S1101021) at Waseda University, and Waseda University Grant for Special Research Projects 2025R-032. The CALET effort in Italy is supported by ASI under Agreement No. 2013-018-R.0 and its amendments. The CALET effort in the United States is supported by NASA through Grants No. NNX16AB99G, No. NNX16AC02G, and No. NNH14ZDA001N-APRA-0075.

References

[1] T. Kobayashi, Y. Komori, K. Yoshida, J. Nishimura, *Astrophys. J.* **601**, 340 (2004).

[2] O. Adriani, *et al.* (CALET Collaboration), *Phys. Rev. Lett.* **131**, 191001 (2023).

[3] J. Alstott, E. Bullmore, D. Plenz, *PLoS One* **9**, 5777 (2014).

[4] S. S. Wilks, *The annals of mathematical statistics* **9**, 60 (1938).

[5] H. Motz, Y. Akaike, *et al.* (CALET collaboration), *PoS* **ICRC2025** (2025). In press.

[6] R. N. Manchester, G. B. Hobbs, A. Teoh, M. Hobbs, *Astron.J.* **129**, 1993 (2005).

[7] D. Gaggero, *et al.*, *Phys.Rev.Lett.* **111**, 021102 (2013).

[8] M. Aguilar, *et al.* (AMS Collaboration), *Phys. Rev. Lett.* **122**, 041102 (2019).

[9] H. Motz, *et al.* (CALET collaboration), *PoS* **ICRC2021**, 100 (2021).

[10] H. Motz, *PoS* **ICRC2023**, 068 (2023).

Full Author List: CALET Collaboration

O. Adriani[1,2], Y. Akaike[3,4], K. Asano[5], Y. Asaoka[5], E. Berti[2,6], P. Betti[2,6], G. Bigongiari[7,8], W.R. Binns[9], M. Bongi[1,2], P. Brogi[7,8], A. Bruno[10], N. Cannady[11], G. Castellini[6], C. Checchia[7,8], M.L. Cherry[12], G. Collazuol[13,14], G.A. de Nolfo[10], K. Ebisawa[15], A.W. Ficklin[12], H. Fuke[15], S. Gonzi[1,2,6], T.G. Guzik[12], T. Hams[16], K. Hibino[17], M. Ichimura[18], M.H. Israel[9], K. Kasahara[19], J. Kataoka[20], R. Kataoka[21], Y. Katayose[22], C. Kato[23], N. Kawanaka[24,25], Y. Kawakubo[26], K. Kobayashi[3,4], K. Kohri[25,27], H.S. Krawczynski[9], J.F. Krizmanic[11], P. Maestro[7,8], P.S. Marrocchesi[7,8], M. Mattiazzi[13,14], A.M. Messineo[8,28], J.W. Mitchell[11], S. Miyake[29], A.A. Moiseev[11,30,31], M. Mori[32], N. Mori[2], H.M. Motz[33], K. Munakata[23], S. Nakahira[15], J. Nishimura[15], M. Negro[12], S. Okuno[17], J.F. Ormes[34], S. Ozawa[35], L. Pacini[2,6], P. Papini[2], B.F. Rauch[9], S.B. Ricciarini[2,6], K. Sakai[36], T. Sakamoto[26], M. Sasaki[11,30,31], Y. Shimizu[17], A. Shiomi[37], P. Spillantini[1], F. Stolzi[7,8], S. Sugita[26], A. Sulaj[7,8], M. Takita[5], T. Tamura[17], T. Terasawa[5], S. Torii[3], Y. Tsunesada[38,39], Y. Uchihori[40], E. Vannuccini[2], J.P. Wefel[12], K. Yamaoka[41], S. Yanagita[42], A. Yoshida[26], K. Yoshida[19], and W.V. Zober[9]

[1]Department of Physics, University of Florence, Via Sansone, 1 - 50019, Sesto Fiorentino, Italy, [2]INFN Sezione di Firenze, Via Sansone, 1 - 50019, Sesto Fiorentino, Italy, [3]Waseda Research Institute for Science and Engineering, Waseda University, 17 Kikuicho, Shinjuku, Tokyo 162-0044, Japan, [4]Space Environment Utilization Center, Human Spaceflight Technology Directorate, Japan Aerospace Exploration Agency, 2-1-1 Sengen, Tsukuba, Ibaraki 305-8505, Japan, [5]Institute for Cosmic Ray Research, The University of Tokyo, 5-1-5 Kashiwa-no-Ha, Kashiwa, Chiba 277-8582, Japan, [6]Institute of Applied Physics (IFAC), National Research Council (CNR), Via Madonna del Piano, 10, 50019, Sesto Fiorentino, Italy, [7]Department of Physical Sciences, Earth and Environment, University of Siena, via Roma 56, 53100 Siena, Italy, [8]INFN Sezione di Pisa, Polo Fibonacci, Largo B. Pontecorvo, 3 - 56127 Pisa, Italy, [9]Department of Physics and McDonnell Center for the Space Sciences, Washington University, One Brookings Drive, St. Louis, Missouri 63130-4899, USA, [10]Heliospheric Physics Laboratory, NASA/GSFC, Greenbelt, Maryland 20771, USA, [11]Astroparticle Physics Laboratory, NASA/GSFC, Greenbelt, Maryland 20771, USA, [12]Department of Physics and Astronomy, Louisiana State University, 202 Nicholson Hall, Baton Rouge, Louisiana 70803, USA, [13]Department of Physics and Astronomy, University of Padova, Via Marzolo, 8, 35131 Padova, Italy, [14]INFN Sezione di Padova, Via Marzolo, 8, 35131 Padova, Italy, [15]Institute of Space and Astronautical Science, Japan Aerospace Exploration Agency, 3-1-1 Yoshinodai, Chuo, Sagamihara, Kanagawa 252-5210, Japan, [16] Center for Space Sciences and Technology, University of Maryland, Baltimore County, 1000 Hilltop Circle, Baltimore, Maryland 21250, USA, [17]Kanagawa University, 3-27-1 Rokkakubashi, Kanagawa, Yokohama, Kanagawa 221-8686, Japan, [18]Faculty of Science and Technology, Graduate School of Science and Technology, Hirosaki University, 3, Bunkyo, Hirosaki, Aomori 036-8561, Japan, [19]Department of Electronic Information Systems, Shibaura Institute of Technology, 307 Fukasaku, Minuma, Saitama 337-8570, Japan, [20]School of Advanced Science and Engineering, Waseda University, 3-4-1 Okubo, Shinjuku, Tokyo 169-8555, Japan, [21] Okinawa Institute of Science and Technology, 1919-1 Tancha, Onna-son, Kunigami-gun Okinawa 904-0495, Japan, [22]Faculty of Engineering, Division of Intelligent Systems Engineering, Yokohama National University, 79-5 Tokiwadai, Hodogaya, Yokohama 240-8501, Japan, [23]Faculty of Science, Shinshu University, 3-1-1 Asahi, Matsumoto, Nagano 390-8621, Japan, [24]Department of Physics, Graduate School of Science, Tokyo Metropolitan University , 1-1 Minamii-Osawa, Hachioji, Tokyo 192-0397, Japan, [25]National Astronomical Observatory of Japan, 2-21-1 Osawa, Mitaka, Tokyo 181-8588, Japan, [26]Department of Physical Sciences, College of Science and Engineering, Aoyama Gakuin University, 5-10-1 Fuchinobe, Chuo, Sagamihara, Kanagawa 252-5258, Japan, [27]Institute of Particle and Nuclear Studies, High Energy Accelerator Research Organization, 1-1 Oho, Tsukuba, Ibaraki 305-0801, Japan, [28]University of Pisa, Polo Fibonacci, Largo B. Pontecorvo, 3 - 56127 Pisa, Italy, [29]Department of Electrical and Electronic Systems Engineering, National Institute of Technology (KOSEN), Gifu College, 2236-2 Kamimakuwa, Motosu-city, Gifu 501-0495, Japan, [30]Center for Research and Exploration in Space Sciences and Technology, NASA/GSFC, Greenbelt, Maryland 20771, USA, [31]Department of Astronomy, University of Maryland, College Park, Maryland 20742, USA, [32]Department of Physical Sciences, College of Science and Engineering, Ritsumeikan University, Shiga 525-8577, Japan, [33]Faculty of Science and Engineering, Global Center for Science and Engineering, Waseda University, 3-4-1 Okubo, Shinjuku, Tokyo 169-8555, Japan, [34]Department of Physics and Astronomy, University of Denver, Physics Building, Room 211, 2112 East Wesley Avenue, Denver, Colorado 80208-6900, USA, [35]Quantum ICT Advanced Development Center, National Institute of Information and Communications Technology, 4-2-1 Nukui-Kitamachi, Koganei, Tokyo 184-8795, Japan, [36]Kavli Institute for Cosmological Physics, The University of Chicago, 5640 South Ellis Avenue, Chicago, IL 60637, USA, [37]College of Industrial Technology, Nihon University, 1-2-1 Izumi, Narashino, Chiba 275-8575, Japan, [38]Graduate School of Science, Osaka Metropolitan University, Sugimoto, Sumiyoshi, Osaka 558-8585, Japan, [39]Nambu Yoichiro Institute for Theoretical and Experimental Physics, Osaka Metropolitan University, Sugimoto, Sumiyoshi, Osaka 558-8585, Japan, [40]National Institutes for Quantum and Radiation Science and Technology, 4-9-1 Anagawa, Inage, Chiba 263-8555, Japan, [41]Nagoya University, Furo, Chikusa, Nagoya 464-8601, Japan, [42]College of Science, Ibaraki University, 2-1-1 Bunkyo, Mito, Ibaraki 310-8512, Japan.

PoS(ICRC2025)099